*photonics*

Article

# Conversion and Active Control between BIC and Absorber in Terahertz Metasurface

**Zhou Xi [1] and Zhencheng Chen [1,2,3,4,*]**

1 School of Electronic and Automation, Guilin University of Electronic and Technology, Guilin 541004, China; xizhou0808@163.com
2 School of Life and Environmental Sciences, Guilin University of Electronic Technology, Guilin 541004, China
3 Guangxi Human Physiological Information Non Invasive Detection Engineering Technology Research Center, Guilin 541004, China
4 Guangxi Colleges and Universities Key Laboratory of Biomedical Sensing and Intelligent Instrument, Guilin 541004, China
* Correspondence: chenzhcheng@163.com

**Abstract:** A multifunctional switchable metamaterial device based on graphene, a gold layer, polyimide, vanadiµm dioxide ($VO_2$), and the sapphire substrate is designed in this paper. The top layer consists of a gold wire, graphene, and two split-ring resonators with the same parameters. By adjusting the Fermi level of graphene, the regulation of BIC and quasi-BIC is realized, and the conversion between BIC and absorber is realized by adjusting the conductivity of $VO_2$. When the device is converted into a wave-absorbing device with single-band absorption characteristics, the Fermi level of graphene at this time is 0.001 eV, the absorption peak at 0.820 THz is higher than 99.5%, and when the Fermi level of regulated graphene is 1 eV, the absorption peak at 0.667 THz is also higher than 99.5%. The peak frequency of the device is 0.640 THz when it converts to quasi-BIC. To the best of our knowledge, this is the first time that the conversion and regulation of BIC and absorber have been achieved using these two phase change materials. Moreover, by adjusting the parameters of the metamaterial structure, the working efficiency and frequency of BIC and absorber can be dynamically adjusted. The electric field distribution and surface current of metamaterials are further studied, and the physical mechanism of effective absorption and BIC is discussed. These results show that the metamaterials proposed in this paper have many advantages, such as terahertz absorption, BIC, and active device control, and are of great significance for developing terahertz multifunctional devices.

**Keywords:** multifunctional metamaterial; BIC; absorber; $VO_2$; graphene

check for updates

**Citation:** Xi, Z.; Chen, Z. Conversion and Active Control between BIC and Absorber in Terahertz Metasurface. *Photonics* **2024**, *11*, 437. https://doi.org/10.3390/photonics11050437

Received: 16 April 2024
Revised: 1 May 2024
Accepted: 5 May 2024
Published: 8 May 2024



## 1. Introduction

The terahertz frequency range spans from 0.1 to 10 THz in the electromagnetic spectrum and is characterized by low energy, wide bandwidth, and high transmittance to non-polar objects [1]. Metamaterials, as periodically structured sub-wavelength composites, exhibit unique electromagnetic properties absent in natural materials and find widespread application in research domains such as security detection, biosensing, wireless communication, and medical imaging [2]. At the same time, metasurface, as a two-dimensional metamaterial with a thickness much smaller than the operating wavelength, can be designed to optimize the structure to achieve terahertz wave modulation [3–5]. Leveraging artificially designed composite metasurface structures, efficient modulation of electromagnetic wave phase, amplitude, and polarization is achievable [6–9]. However, since the properties of the traditional metasurface are fixed after machining, the traditional metasurface has no active modulation capability and no multifunctional conversion capability. Therefore, the design and research of multifunctional terahertz devices by incorporating phase change materials into the design of metasurface has become one of the research hotspots, including perfect absorption, polarization conversion, continuous domain bound states (BIC), and so on [10–16].

The concept of BIC originated from quantum systems. However, quantum experimental systems are often prohibitively expensive and complex. Therefore, the flexibility of metasurface design and the modulation of electromagnetic waves offer a promising platform for studying BIC [17–19]. There are two main coupling ways to achieve BIC in metasurfaces: The first method is the coupling between two structures to produce a BIC. This coupling usually produces a quasi-BIC peak by breaking the symmetry between structures, i.e., by adjusting one of the structural parameters [20–24]. The BIC generated by such structures is called the BIC of symmetry protection [25–29]. Another kind, although it is composed of two symmetric structures, the nature of its generation of BIC for the two modes (electric dipole and magnetic dipole) between the mutual coupling, that is, in the process of changing the structural parameters, always maintains the symmetry of the hypersurface structure is not broken [30–34]. When the BIC phenomenon occurs under certain structural parameters, the Fano peak disappears, and the BIC pattern produced by such structures is called accidental BIC [35]. In recent years, numerous research papers on BIC devices and absorbers have been published successively [36–39]. With the continuous research and discovery of researchers, only focusing on the tunability of a single function, such as a single absorption characteristic or a single BIC device, cannot meet the actual needs. Therefore, researchers have utilized phase change materials such as $VO_2$ and graphene, among others, to engineer terahertz devices with multifunctionality. Vanadium dioxide ($VO_2$) serves as a foundational material undergoing a remarkable transition from an insulating phase to a metallic phase at 68 °C [40–45]. This phase transition results in a significant alteration in electrical conductivity. Graphene can adjust the Fermi level to adjust the graphene insulation state to the metal state. Therefore, the multifunctional control of the device can be realized by adjusting the properties of the phase change material. Ranjan Singh et al. produced a Fano peak with a high Q value by breaking the symmetry of the structure [46]. Silvia Romano et al. utilized photonic crystals to generate quasi-BIC peaks with high Q-values, enabling high-sensitivity sensing detection of biological cells [47]. Guozheng Wu et al. used a vanadium dioxide ($VO_2$) resonance structure to achieve a metamaterial absorber with a simple structure [48]. Ruyuan Zheng et al. utilized a single layer of graphene to combine patterns, achieving a very simple terahertz-absorbing material [49]. With the rapid advancement of practical applications, single-function devices cannot meet the growing demand, leading to increased attention on the research of multifunctional devices. Huihui Jing et al. proposed a bi-functional metamaterial device based on vanadium dioxide ($VO_2$), achieving an absorption rate of more than 90% [50]. Jitao Li et al. introduced graphene into the BIC metasurface and realized the control of quasi-BIC and BIC by adjusting the Fermi level of graphene [51]. Gao et al. proposed a bi-functional metasurface with a maximum absorption rate of 90.3% and generated a secondary Fano-like structure [52]. Li et al. proposed two dual-function terahertz switchable metasurfaces, exhibiting absorption rates exceeding 90% and producing Fano-like structures [53]. As far as we know, most of the devices designed in the reported papers can realize switching between absorption and Fano-like effects or quasi-BIC and BIC effect functions, but the design of metasurface structures satisfying both functions has yet to be reported. However, the device designed in this paper not only has the above-mentioned two types of switching functions but also can realize the metasurface with efficient absorption and BIC regulation functions, which can greatly improve the adjustability and practicability of the device in practical applications and has the potential application prospects in other terahertz fields.

In this paper, an efficient tunable dual-function terahertz device is proposed. By introducing phase change materials into the device, we achieve not only the conversion from an absorber to a BIC device but also the transition between BIC and quasi-BIC states, and high absorptivity and excellent tunability are achieved. When $VO_2$ is converted from an insulating state to a metallic state, and the Fermi levels of graphene are 0.001 eV and 1 eV, respectively, the absorption efficiency is above 99.5% at 0.820 THz and 0.667 THz.

Secondly, by adjusting the Fermi level of graphene, we achieve dynamic regulation from BIC to quasi-BIC. Furthermore, we also studied and analyzed the influence of structural parameter changes on the performance of the device. The proposed structure is significant in biosensors, imaging, and multifunctional terahertz devices.

## 2. Design and Methods

We used the CST Microwave Studio to conduct numerical simulations using a frequency domain solver to investigate the transmission and absorption properties of the structure. The proposed structure diagram is shown in Figure 1. The unit structure period is 240 µm, the outer diameter $R_1$ of the top ring is 100 µm, the inner diameter $R_2$ is 80 µm, and the linear distance $g_2$ between the opening of the upper and lower half rings is 20 µm. The CW structure in the middle of the ring is composed of gold and graphene material; the length of the graphene $g_1$ is 36 µm, and the lengths of the two gold CW are the same. As shown in Figure 1a, the structure has a total of four layers, from top to bottom, which are patterned metal and graphene, polyimide, $VO_2$ film, and sapphire substrate. Among them, the relative dielectric constants of sapphire, polyimide, and $VO_2$ (thickness t is 1.2 µm) are 9.67, 3.1, and 9, respectively, and the polyimide loss tan $\delta = 0.07$. The thickness of the top metal is 0.2 µm, the polyimide thickness $h_2$ is 20 µm, and the sapphire thickness $h_1$ is 50 µm.

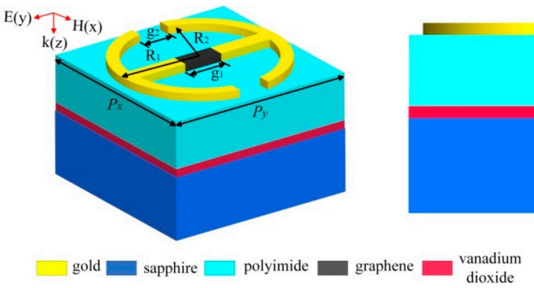


(**a**)


(**b**)

**Figure 1.** (**a**) Schematic of the metamaterial composed of Au and graphene–polyimide–$VO_2$–sapphire multilayer. Parameters: $h_2$ = 20 µm, t = 1.2 µm, $h_1$ =50 µm. (**b**) Top view of metamaterial unit cell with parameters: $P_y = P_x$ = 240 µm, $g_1$ = 36 µm, $g_2$ =20 µm, $R_1$ = 100 µm, $R_2$ = 80 µm.

## 3. The Performance of BIC Conversion to Quasi-BIC

When the conductivity of $VO_2$ is 10 S/m, the transmission spectrum of the whole structure is shown in Figure 2a. As shown in Figure 2b, we can know from the surface current diagram that the quasi-BIC peak of the structure is generated by the coupling of a magnetic dipole and an electric dipole, and the two modes are excited simultaneously at the quasi-BIC frequency, so that they can be regarded as two bright modes.

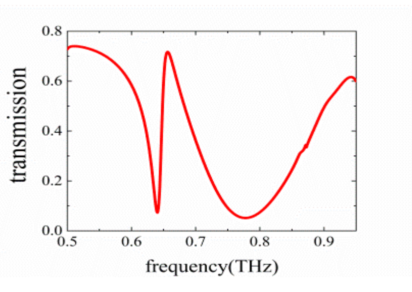


(**a**)

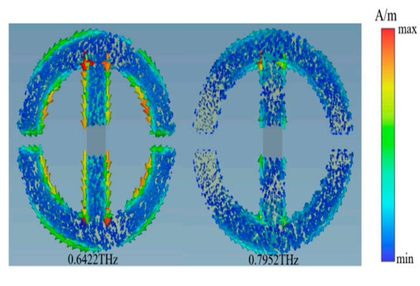


(**b**)

**Figure 2.** (**a**) When the $VO_2$ conductivity is 10 S/m, the transmission spectral line of the entire structure. (**b**) Surface current distribution diagram of metasurface structure.

Based on the coupled mode theory, the expression of mutual coupling between two bright modes is as follows:

$$\begin{pmatrix} \omega - \omega_a - i\gamma_a & \Omega \\ \Omega & \omega - \omega_b - i\gamma_b \end{pmatrix} \begin{pmatrix} a \\ b \end{pmatrix} = \begin{pmatrix} \sqrt{\gamma_a}E \\ \sqrt{\gamma_b}e^{i\phi}E \end{pmatrix} \tag{1}$$

$$\Omega = g - i\sqrt{\gamma_a\gamma_b}e^{i\phi} \tag{2}$$

The parameter $\omega$ represents the frequency of the incident electromagnetic wave, whose amplitude is represented by $E$; $\omega_a$ and $\omega_b$ represent the resonant frequencies of the two open-mode structures, respectively. The non-diagonal term $\Omega$ in the matrix represents the lossy coupling strength. The parameters g represents the coupling strength between the two bright modes, and $\gamma_a$ and $\gamma_b$ represent the loss of the two bright modes, respectively. The physical quantity $\phi$ is phase information, which can be calculated from the phase corresponding to the resonant frequency of a single bright mode, i.e., $\phi = \phi_1 - \phi_2$.

By solving Equation (1), we can obtain the metasurface structure's energy amplitude $a$ and $b$. The expressions for $a$ and $b$ are as follows:

$$a = \frac{(\sqrt{\gamma_a}(\omega - \omega_b - i\gamma_b) - \Omega\sqrt{\gamma_b}e^{i\phi})E}{(\omega - \omega_a - i\gamma_a)(\omega - \omega_b - i\gamma_b) - \Omega^2} \tag{3}$$

$$b = \frac{(\sqrt{\gamma_b}(\omega - \omega_a - i\gamma_a) - \Omega\sqrt{\gamma_a})E}{(\omega - \omega_a - i\gamma_a)(\omega - \omega_b - i\gamma_b) - \Omega^2} \tag{4}$$

Then the effective electrical polarizability of the entire metasurface structure can be calculated according to Formula (5).

$$\chi_{eff} = \frac{\sqrt{\gamma_a}a + \sqrt{\gamma_b}e^{i\phi}b}{\varepsilon_0 E} \tag{5}$$

$\chi_{eff}$ represents the effective electrical polarizability of the metasurface structure, which is obtained by linear superposition of the energy amplitudes $a$ and $b$. $\varepsilon_0$ represents the dielectric constant in a vacuum, with a value of magnitude 1.

Finally, the transmission spectral line can be obtained according to Formula (6).

$$T \approx 1 - \mathrm{Im}(\chi_{eff}) \approx 1 - \mathrm{Im}(\frac{(\omega - \omega_b - i\gamma_b)\gamma_b e^{2i\phi} + (\omega - \omega_b - i\gamma_b)\gamma_a - 2\Omega\sqrt{\gamma_a\gamma_b}e^{i\phi}}{(\omega - \omega_a - i\gamma_a)(\omega - \omega_b - i\gamma_b) - \Omega^2}) \tag{6}$$

As shown in Figure 3a, when $VO_2$ is in a nonmetallic state, BIC can be regulated by regulating the Fermi level of graphene. When the Fermi level of graphene is 0.001 eV, there is no resonance peak at 0.59–0.65 THz, and the transmission of terahertz waves is greater than 0.62. When the Fermi level of graphene increases, the transmission spectrum of the device will change correspondingly; the Fano peak (quasi-BIC peak) is produced in the 0.59 to 0.65 THz interval, and the transmittance drops sharply in this resonant interval. It can be seen from the above analysis that the device designed in this paper can regulate the resonance frequency and amplitude by changing the Fermi level of graphene. In order to further discuss the coupling effect of this structure, we discuss the effects of changes in graphene length $g_1$, ring outer diameter $R_1$, ring inner diameter $R_2$, ring opening $g_2$, and PI thickness $h_2$.

As shown in Figure 3b, when the length of graphene increases, the transmittance increases, the Fano peak gradually disappears, and the adjustment of $g_1$ can also improve the Q value of the structure. As shown in Figure 3c, when the outer diameter of the ring increases, the interaction between the structures is enhanced, the distance between the two resonant peaks gradually increases, and the peak value slowly decreases. At the same time, the increase in the whole structure's metal area will cause the system's loss to increase, and the half-height full width will become wider. As shown in Figure 3d, on the contrary, when the inner diameter of the ring increases, the peak value slowly decreases, the distance between the two peaks decreases, and the half-height full width gradually decreases. As shown in Figure 3e, when the ring opening becomes larger, the transmittance increases slowly, and the resonant frequency moves slowly to the high frequency. As shown in Figure 3f, when the thickness of the polyimide increases, the peak value is almost unchanged, and the resonant frequency slowly moves to the high frequency.

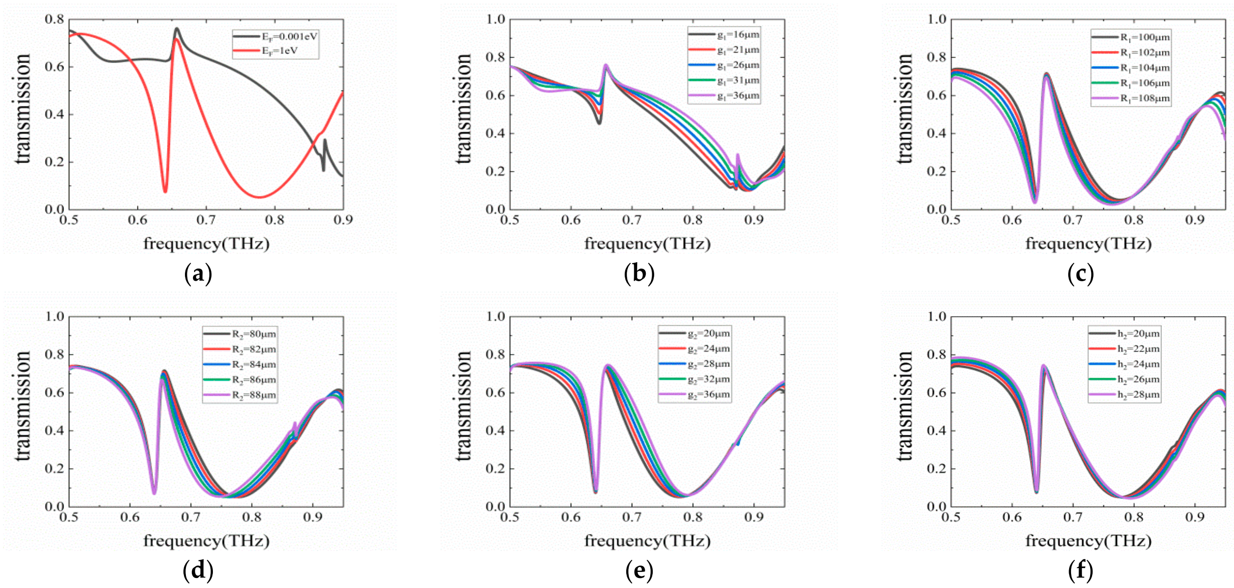


**Figure 3.** (**a**) Transmission spectra of different Fermi levels of graphene. (**b**) Transmission spectra of different graphene lengths (the graphene Fermi level is 0.001 eV). (**c**) Transmission spectrum with different outer radius of the ring (the graphene Fermi level is 1 eV). (**d**) Transmission spectrum with different inner ring radius (the graphene Fermi level is 1 eV). (**e**) Transmission spectrum of different ring openings (the graphene Fermi level is 1 eV). (**f**) Transmission spectra of different polyimide thicknesses (the graphene Fermi level is 1 eV).

## 4. Performance of BIC Transabsorbers

In practical applications, the absorber is also an important functional device, so we analyze and discuss the performance of the absorber. We compared the influence of structural parameters on BIC and the influence of structural parameters on the absorber. Through analysis, we found that the influence of changing structural parameters on the BIC is small, and the influence on the absorption of the absorber is larger. Therefore, in this section, we only discuss the variation in the absorption spectrum of the absorber, i.e., the case of $VO_2$ conductivity of $2 \times 10^5$ S/m. (that is when the $VO_2$ layer is in a metallic state). When the temperature change causes $VO_2$ to be in a metallic state, its structure transforms into a metal-media-metal-like structure. This transformation produces an absorption peak of over 99.5% at 0.667 THz, enabling efficient single-band absorption. The specific simulation effect of the model is shown in Figure 4a.

As shown in Figure 4b, when the Fermi level of graphene increases, the resonant frequency becomes smaller, the absorption efficiency is more than 99.5%, and the absorption bandwidth changes from 0.05 THz to 0.02 THz. As shown in Figure 4c, when the thickness of polyimide increases, the resonant frequency moves to the low frequency, and the absorption efficiency of the absorption peak decreases with the increase in $h_2$, so the optimal thickness of polyimide is determined to be 20 μm. At this time, the entire metasurface structure meets the impedance matching condition, and the equivalent refractive index meets the real part of 1 and the imaginary part of 0. As shown in Figure 4d, when the radius of the ring $R_1$ increases, the resonant frequency moves to the low frequency, and the absorption efficiency of the absorption peak decreases with the increase in $R_1$, but the amplitude of each reduction is small, so the radius of the ring is selected to 100 μm for the best absorption effect. As shown in Figure 4e, when the inner diameter $R_2$ of the ring increases, the resonant frequency moves to the low frequency, and the absorption efficiency of the absorption peak decreases with the increase in $R_2$. As shown in Figure 4f, when the ring opening $g_2$ becomes larger, the resonant frequency moves to the high frequency, and the absorption efficiency of the absorption peak decreases with the increase in $g_2$.

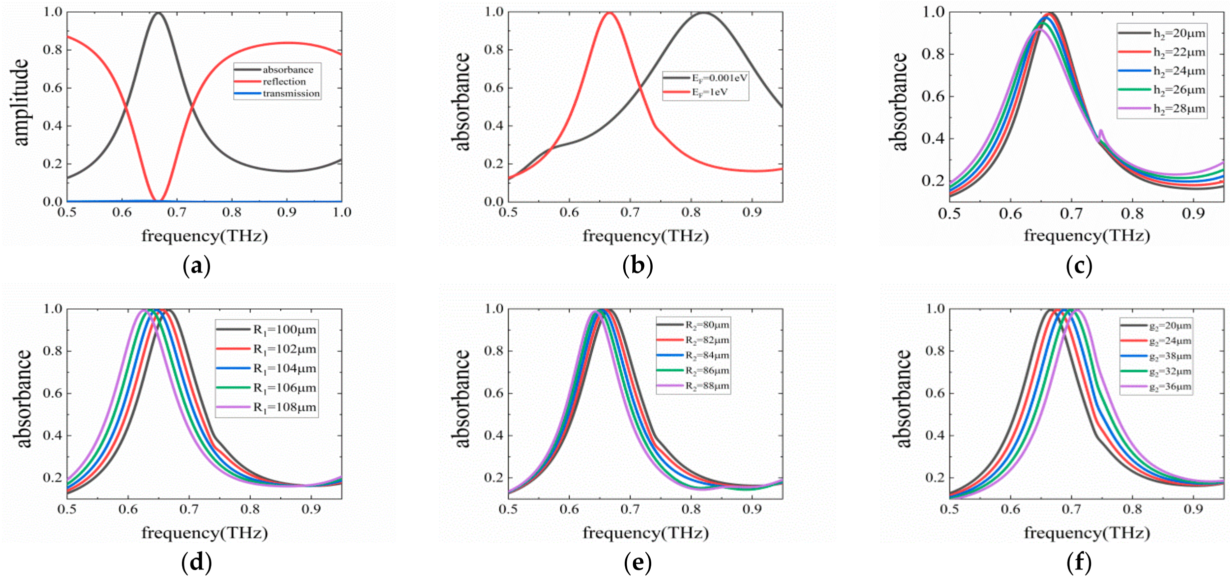


**Figure 4.** (**a**) When the $VO_2$ conductivity is 200,000 S/m, the absorption (black line), reflection (red line), and transmission (blue line) of the metal-dielectric-metal-like structure absorber. (**b**) Absorbance spectra of different Fermi levels of graphene. (**c**) Absorbance spectra of different polyimide thicknesses. (**d**) Absorbance spectra with different outer radii of the ring. (**e**) Absorbance spectra with different inner radii of the ring. (**f**) Absorbance spectra of different ring openings.

Then, we further study the influence of structural parameters on the absorber, and we discuss the influence of the structure period size on the absorption efficiency. As shown in Figure 5a, when the period length $P_x$ increases, the peak value of the absorption peak slowly decreases, and the resonant frequency moves to the high frequency. It can be seen from Figure 5b that when the period length $P_y$ increases, the peak value of the absorption peak decreases slowly, and the resonant frequency moves to the low frequency. Through the analysis of simulation experiments, we can think that the absorption efficiency of the structure does not change significantly when the period length is changed, which is a very important phenomenon. Therefore, combined with the above parameter change experiment, we can generate resonance absorption of specific frequencies by adjusting structural parameters. We can also optimize the parameters of the geometry to improve the absorption efficiency. Furthermore, we can also change the scale of the metasurface structure to extend it to other frequency bands.

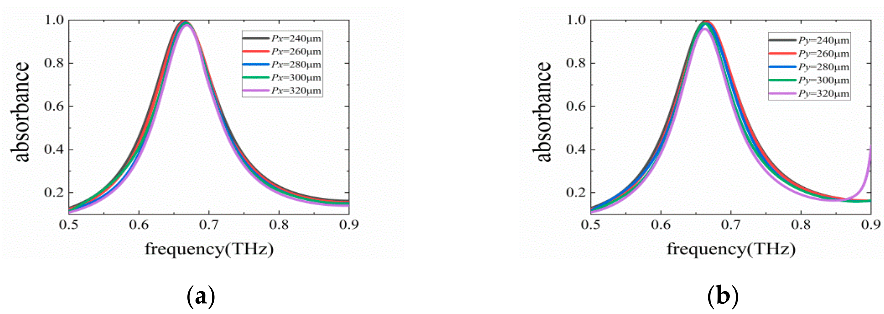


**Figure 5.** Absorbance spectrum with a single parameter change at a $VO_2$ conductivity of 200,000 S/m. (**a**) Absorbance spectra of different period lengths $P_x$. (**b**) Absorbance spectra of different period lengths $P_y$.

## 5. Discussion

The BIC generation mechanism in this paper is generated by the coupling of an electric dipole and a magnetic dipole. When the resonant frequencies corresponding to the two polarons are the same ($\omega_a = \omega_b$), the phase of the two polarons is the same, so the leakage waves of the two structures will interfere with each other in the far field and cancel each other, resulting in the BIC effect. When $g_1$ is changed, the resonant frequency $\omega_a$ of the electric dipole will change, and the phase will also change so that the leakage wave cannot be altogether canceled out, resulting in a quasi-BIC effect. When $g_2$ is changed, the resonant frequency of the magnetic dipole is changed, that is, the parameter $\omega_b$ in the coupling mode equation. The parameters $\gamma_a$ and $\gamma_b$ in the coupled mode equation correspond to the line width of the hypersurface structure. When the line width narrows, the loss of the structure will decrease in response.

Under the existing processing technology, switching and tunable broadband terahertz absorption based on graphene and vanadium dioxide has been fabricated using deposition, chemical vapor deposition, wet transfer technology, gas equivalent ionization etching technology, and magnetron sputtering deposition technology [54]. Switching and tunable wideband terahertz absorption based on graphene and vanadium dioxide has been achieved using thermal evaporation systems, spin coating and ground curing processes, magnetron sputtering, and wet transfer techniques [55]. Using atomic layer deposition (ALD) technology and lithographic electron beam lithography (EBL) technology, EBL technology has achieved a tunable multi-band metamaterial coherently perfect absorber based on graphene and vanadium dioxide [56]. With the continuous maturity and improvement of processing technology, terahertz devices with multiple functions can be successfully processed, laying the foundation for the future sustainable development of multifunctional devices.

## 6. Conclusions

In this study, a novel and multifunctional metasurface is proposed. By controlling two phase change materials, graphene and vanadium dioxide ($VO_2$), we achieve the regulation of BIC and quasi-BIC, as well as the switching and transformation of the absorber and BIC. By adjusting the Fermi level of graphene, we can effectively regulate the conversion between BIC and quasi-BIC. Secondly, when we actively raise the temperature, $VO_2$ changes from an insulating state to a metallic state, and the structure designed in this paper changes from BIC to an absorber. In addition, the mechanism of the proposed structure is analyzed using the current distribution. The effects of different functions of the metasurface are discussed by changing the different structural parameters of the metasurface, which is of great significance for developing terahertz devices in the future. These findings provide some potential applications for studying terahertz absorption, polarization conversion, modulation, and imaging.

**Author Contributions:** Conceptualization, Z.X.; Data curation, Z.X. and Z.C.; Formal analysis, Z.X.; Funding acquisition, Z.X.; Investigation, Z.X. and Z.C.; Methodology, Z.X. and Z.C.; Supervision, Z.X.; Writing—original draft, Z.X.; Writing—review and editing, Z.X. and Z.C. All authors have read and agreed to the published version of the manuscript.

**Funding:** This research was funded by the Guangxi Innovation Driven Development Project grant number [No. 2019AA12005] and the National Natural Science Foundation of China Joint Fund Priority Program grant number [No. U22A2092].

**Institutional Review Board Statement:** Not applicable.

**Informed Consent Statement:** Not applicable.

**Data Availability Statement:** The raw data are available upon request from the authors.

**Conflicts of Interest:** The authors declare no conflicts of interest.

## References


1. Li, C.Q.; Song, Z.Y. Tailoring terahertz wavefront with state switching in $VO_2$ Pancharatnam–Berry metasurfaces. *Opt. Laser Technol.* **2023**, *157*, 108764. [CrossRef]
2. Mei, J.S.; Song, C.L.; Shu, C. Active manipulation of dual transparency windows in dark–bright–dark mode coupling graphene metamaterial. *Opt. Commun.* **2021**, *488*, 126851. [CrossRef]
3. Zhao, H.L.; Ren, Y.; Fang, L.; Lin, H. Electromagnetic induced transparency in graphene waveguide structure for Terahertz application. *Results Phys.* **2020**, *16*, 102971. [CrossRef]
4. Chen, Z.; Chen, Z.H.; Tang, H.W.; Shen, T.; Zhang, H. Dual-tunable and high-efficiency multifunctional terahertz device based on black phosphorus and graphene metasurface. *Opt. Mater.* **2024**, *149*, 115065. [CrossRef]
5. Yin, Y.J.; Lv, Y.; Sun, Y.Z.; Zhang, H.F. Tunable conversion of electromagnetically induced transparency to electromagnetically induced absorption based on vanadium dioxide metastructure. *Optik* **2024**, *296*, 171554. [CrossRef]
6. Hua, J.C. Two-color electromagnetically induced transparency generated slow light in double-mechanical-mode coupling carbon nanotube resonators. *IScience* **2024**, *27*, 109328.
7. Jahan, I.M.; Faruque, I.R.M.; Mugren, A.K. Polarization-incident angle independent metamaterial wave absorber for enhanced electromagnetic energy harvesting in ultraviolet-B, visible spectrum, and near-infrared frequency range. *Mater. Today Commun.* **2024**, *38*, 108229. [CrossRef]
8. Gao, E.; Cao, G.T.; Deng, Y.; Li, H.J.; Chen, X.S.; Li, G.H. Perfect absorption frequency modulation, optical switching and slow-light multifunctional integrated device based on plasmon-induced absorption. *Opt. Laser Technol.* **2024**, *168*, 109840. [CrossRef]
9. Ain, K.; Putra, A.P.; Rahma, O.N.; Hikmawati, D.; Rahmatillah, A.; Rahmatillah, C.A.C. Electrical Impedance Spectroscopy as a Potential Tool for Detecting Bone Porosity. *Sens. Actuators A Phys.* **2024**, *370*, 115252. [CrossRef]
10. Kim, K.H.; Cho, M.C. Tunable multiband circular dichroism and asymmetric transmission enabled by chiral quasi-BICs in dielectric metasurfaces covered with graphene. *Opt. Mater.* **2024**, *148*, 114798. [CrossRef]
11. Wang, T.Y.; Liu, S.Q.; Zhang, J.H.; Xu, L.; Yang, M.Y.; Han, B.; Ma, D.; Jiang, S.J.; Jiao, Q.B.; Tan, X. Highly sensitive polarization-tunable Fano resonant metasurface excited by BICs for refractive index detection. *Results Phys.* **2024**, *58*, 107451. [CrossRef]
12. Wang, Y.; Zhang, D.Z.; Sun, G.C.; Yao, Z.Y.; Zhang, K.; Shi, W. Tunable terahertz bound state in the continuum in graphene metagrating. *Opt. Commun.* **2023**, *541*, 129549. [CrossRef]
13. Liu, C.X.; Liu, W.Y.; Li, W.; Gu, Y.X.; Liu, L.; Zhou, Y.R.; Xing, E.B.; Tang, J.; Liu, J. Design of simple, ultrasensitive, and tunable teraherz metasensors based on quasi-BIC. *Opt. Commun.* **2024**, *550*, 129967. [CrossRef]
14. Zhang, C.; Nie, X.M.; Liu, Z.T.; Chen, Z.M.; Ma, C.Y.; Yue, F.Y.; Wang, L.; He, Z.X. High resolution UV spectral imaging and bio-detection with magnetic dipole quasi-BIC resonant dielectric metasurfaces. *Opt. Commun.* **2023**, *530*, 129173. [CrossRef]
15. Morales, R.C.; Kamali, K.Z.; Xu, L.; Miroshnichenko, A.; Rahmani, M.; Neshev, D. 11—Nonlinear phenomena empowered by resonant dielectric nanostructures. In *Nanophotonics, All-Dielectric Nanophotonics*; Shalin, A.S., Valero, A.C., Miroshnichenko, A., Eds.; Elsevier: Amsterdam, The Netherlands, 2024; pp. 329–364.
16. Shi, W.J.; Wang, Z.L.; Zhang, C.C.; Zhang, C.F.; Li, W.; Liu, H.J. Enhanced optical nonlinearity of epsilon-near-zero metasurface by quasi-bound state in the continuum. *Mater. Today Nano* **2024**, *26*, 100474. [CrossRef]
17. Wang, D.D.; Tian, J.K.; Ma, T.; Zhang, Y.; Yue, S. Terahertz modulators based on $VO_2$–metal hybridized metamaterials for free switching between BIC and quasi-BIC states. *Opt. Commun.* **2024**, *551*, 130040. [CrossRef]
18. Li, X.M.; Feng, H.; Yun, M.J.; Wang, Z.; Hu, Y.G.; Gu, Y.J.; Liu, F.H.; Wu, W.P. Polarization-independent and all-optically modulated multiband metamaterial coherent perfect absorber. *Opt. Laser Technol.* **2023**, *166*, 109644. [CrossRef]
19. Li, J.S.; Xue, Y.Y.; Guo, F.L. Triple frequency bands terahertz metasurface sensor based on EIT and BIC effects. *Opt. Commun.* **2024**, *554*, 130225. [CrossRef]
20. Liu, X.Y.; Li, F.Y.; Li, Y.X.; Tang, T.T.; Liao, Y.L.; Lu, Y.C.; Wen, Q.Y. Terahertz metasurfaces based on bound states in the continuum (BIC) for high-sensitivity refractive index sensing. *Optik* **2022**, *261*, 169248. [CrossRef]
21. Duan, B.; Liu, S.Y.; Liu, X.; Yu, X.C.; Wang, C.; Yang, D.Q. High-Q quasi-BIC in photonic crystal nanobeam for ultrahigh sensitivity refractive index sensing. *Results Phys.* **2023**, *47*, 106304. [CrossRef]
22. Li, X.; Liu, D.; Huo, Y.Y.; Yue, Q.Y.; Ning, T.Y. Low-voltage electro-optic switching and modulation of second harmonic generation in lithium niobate resonant waveguide gratings assisted by quasi-BICs. *Opt. Laser Technol.* **2023**, *160*, 109083. [CrossRef]
23. Li, F.Y.; Li, Y.X.; Tang, T.T.; Liao, Y.L.; Lu, Y.C.; Liu, X.Y.; Wen, Q.Y. Metal-graphene hybrid terahertz metasurfaces based on bound states in the continuum (BIC) and quasi-BIC for dynamic near-field imaging. *J. Alloys Compd.* **2022**, *928*, 167232. [CrossRef]
24. Kim, K.H.; Cho, M.C. Extremely high-Q quasi-BICs induced by simultaneously broken out-of- and in-plane symmetries in dielectric metasurfaces of low-index materials. *Opt. Commun.* **2023**, *535*, 129356. [CrossRef]
25. Ghanekar, A.; Shrewsbury, B.K.; Hsu, C.W.; Kapadia, R.; Povinelli, M.L. Electro-optic symmetry breaking of BIC modes for tunable infrared emissivity. *Mater. Today Phys.* **2023**, *35*, 101113. [CrossRef]
26. Yan, D.X.; Zhao, C.C.; Qiu, Y.; Li, X.J.; Zhang, L.; Li, J.J. Efficient second harmonic generation from nonlinear one-dimensional meta-grating metasurface under vertically incident pump laser excitation. *Infrared Phys. Technol.* **2024**, *136*, 105005. [CrossRef]
27. Qiu, Y.; Zhang, X.; Wang, K.N.; Qian, L.Y. Electrically tunable dual-channel absorber based on a graphene integrated slanted grating cavity. *Opt. Commun.* **2024**, *559*, 130406. [CrossRef]

28. Qiu, Y.; Yan, D.X.; Li, X.J.; Zhang, L.; Li, J.J. Highly efficient second harmonic generation assisted by the quasi-bound states in the continuum from AlGaAs meta-gratings. *Opt. Commun.* **2023**, *546*, 129772. [CrossRef]
29. Tang, L.C.; Chen, J.X.; Tang, T.; Wang, L.; Xiong, Z.G. Actively modulating near-infrared absorption of monolayer graphene in a compound grating-coupled waveguide structure. *Phys. E Low-Dimens. Syst. Nanostructures* **2024**, *158*, 115889. [CrossRef]
30. Hou, B.; Li, Z.Y.; He, L.; Yi, Z.; Song, Q.J.; Yang, H.; Yi, Y.G.; Li, H.L. Enhanced quasi-BIC refractive index sensing based on controlling the Fermi energy of Dirac semimetal metasurface. *Opt. Laser Technol.* **2023**, *164*, 109537. [CrossRef]
31. Zhang, F.L.; Huang, X.C.; Zhao, Q.; Chen, L.; Wang, Y.; Li, Q.; He, X.; Li, C.; Chen, K. Fano resonance of an asymmetric dielectric wire pair. *Appl. Phys. Lett.* **2014**, *105*, 172901. [CrossRef]
32. Lim, W.X.; Singh, R. Universal behaviour of high-Q Fano resonances in metamaterials: Terahertz to near-infrared regime. *Nano Converg.* **2018**, *5*, 5. [CrossRef] [PubMed]
33. Fedotov, V.A.; Rose, M.; Prosvirnin, S.L.; Papasimakis, N.; Zheludev, N.I. Sharp trapped-mode resonances in planar metamaterials with a broken structural symmetry. *Phys. Rev. Lett.* **2007**, *99*, 147401. [CrossRef] [PubMed]
34. Campione, S.; Liu, S.; Basilio, L.I.; Warne, L.K.; Langston, W.L.; Luk, T.S.; Wendt, J.R.; Reno, J.L.; Keeler, G.A.; Brener, L.; et al. Broken symmetry dielectric resonators for high quality factor Fano metasurfaces. *ACS Photonics* **2016**, *32*, 362–2367. [CrossRef]
35. Islam, O.; Anik, M.; Hussayeen, K.; Shakib, S.H.; Niloy, N.H.; Talukder, H.; Biswas, S.K. Bound state in the continuum supported asymmetric dome-shaped dielectric metasurface: Crossing and avoided crossing of transmission with applications. *Opt. Laser Technol.* **2024**, *174*, 110634. [CrossRef]
36. Vabishchevich, P.P.; Liu, S.; Sinclair, M.B.; Keeler, G.A.; Peake, G.M.; Breber, L. Enhanced second-harmonic generation using broken symmetry III–V semiconductor Fano metasurfaces. *ACS Photonics* **2018**, *5*, 1685–1690. [CrossRef]
37. Tuz, V.R.; Khardikov, V.V.; Kupriianov, A.S.; Domina, K.L.; Xu, S.; Wang, H.; Sun, H.B. High-quality trapped modes in all-dielectric metamaterials. *Opt. Express* **2018**, *26*, 2905–2916. [CrossRef] [PubMed]
38. Cen, W.Y.; Lang, T.T.; Wang, J.F.; Xiao, M.Y. High-Q Fano Terahertz resonance based on bound states in the continuum in All-dielectric metasurface. *Appl. Surf. Sci.* **2022**, *575*, 151723. [CrossRef]
39. Zhao, X.G.; Chen, C.X.; Kaj, K.L.; Hammock, L.; Huang, Y.W.; Averitt, R.D.; Zhang, X. Terahertz investigation of bound states in the continuum of metallic metasurfaces. *Optica* **2020**, *7*, 1548–1554. [CrossRef]
40. Wang, Q.; Li, B.X.; Zeng, L.L.; Yang, Q.L.; Zhang, X.J.; Wen, R.Q.; Deng, C.S. Switchable quadruple narrowband to broadband terahertz perfect absorber based on graphene and $VO_2$ metamaterials. *Diam. Relat. Mater.* **2024**, *142*, 110832. [CrossRef]
41. Jia, Y.; Wang, G.; Zhang, X.; Li, M.C.; Miao, F.J.; Gao, Y.C. Terahertz multi-band absorber and dual-bandwidth polarization converter based on $VO_2$ and graphene. *Results Phys.* **2023**, *53*, 107006. [CrossRef]
42. Ri, K.J.; Kim, J.S.; Kim, J.H.; Ri, C.H. Tunable triple-broadband terahertz metamaterial absorber using a single $VO_2$ circular ring. *Opt. Commun.* **2023**, *542*, 129573. [CrossRef]
43. Zhang, L.W.; Liu, W.F.; Cencillo-Abad, P.; Wang, Q.; Huang, X.; Leng, Y.M. A tunable broadband polarization-independent metamaterial terahertz absorber based on $VO_2$ and Dirac semimetal. *Opt. Commun.* **2023**, *542*, 129602. [CrossRef]
44. Duan, G.Y.; Wu, Y.K.; Zhu, H.X.; Zhang, X.Y.; Wang, B.X. Triple-band tunable terahertz metamaterial absorber enabled by surface design of goggles-like structure using two identical $VO_2$ square frames connected by a $VO_2$ horizontal connecting strip. *Results Opt.* **2023**, *10*, 100370. [CrossRef]
45. Ri, K.J.; Ri, C.H. Tunable dual-broadband terahertz metamaterial absorber based on a simple design of slotted $VO_2$ resonator. *Opt. Commun.* **2023**, *536*, 129377. [CrossRef]
46. Singh, R.; Al-Naib, I.A.; Koch, M.; Zhang, M. Sharp Fano resonances in THz metamaterials. *Opt. Express.* **2011**, *19*, 6312–6319. [CrossRef] [PubMed]
47. Romano, S.; Mangini, M.; Penzo, E.; Cabrini, S.; De Luca, A.C.; Rendina, I.; Zito, G. Ultrasensitive surface refractive index imaging based on quasi-bound states in the continuum. *ACS Nano* **2020**, *14*, 15417–15427. [CrossRef] [PubMed]
48. Wu, G.Z.; Li, C.; Wang, D.; Gao, S.; Chen, W.Y.; Guo, S.J.; Xiong, J.R. Vanadium dioxide-based ultra-broadband metamaterial absorber for terahertz waves. *Opt. Mater.* **2024**, *147*, 114667. [CrossRef]
49. Zheng, R.Y.; Liu, Y.H.; Ling, L.; Sheng, Z.X.; Yi, Z.; Song, Q.J.; Tang, B.; Zeng, Q.D.; Chen, J.; Sun, T.Y. Ultra wideband tunable terahertz metamaterial absorber based on single-layer graphene strip. *Diam. Relat. Mater.* **2024**, *141*, 110713. [CrossRef]
50. Jing, H.H.; Kang, J.F.; Song, C.W.; Duan, J.P.; Qu, Z.; Wang, J.Y.; Zhang, B.Z. Bifunctional switchable terahertz metamaterial in the same operating band based on $VO_2$. *Opt. Commun.* **2024**, *552*, 130047. [CrossRef]
51. Li, J.T.; Li, J.; Zheng, C.; Yue, Z.; Wang, S.; Li, M.; Yao, J. Free switch between bound states in the continuum (BIC) and quasi-BIC supported by graphene-metal terahertz metasurfaces. *Carbon* **2021**, *182*, 506–515. [CrossRef]
52. Gao, C.J.; Zhang, H.F. Switchable metasurface with electromagnetically induced transparency and absorption simultaneously realizing circular polarization-insensitive circular-to-linear polarization conversion. *Ann. Phys.* **2022**, *534*, 2200108. [CrossRef]
53. Li, W.; Qu, Z.; Duan, J.P.; Wang, J.Y.; Kang, J.F.; Yao, B.Y.; Zhang, B.Z. Switchable dual-function metasurfaces with electromagnetic induction transparency-like and absorption. *Optik* **2023**, *272*, 170343. [CrossRef]
54. Li, D.Z.; He, S.; Su, L.; Du, H.T.; Tian, Y.; Gao, Z.Q.; Xie, B.; Huang, G.Q. Switchable and tunable terahertz metamaterial absorber based on graphene and vanadium dioxide. *Opt. Mater.* **2024**, *147*, 114655. [CrossRef]

55. Wang, X.W.; Xiao, Z.Y.; Zheng, Q. Switchable and tunable broadband terahertz absorption, linear polarization conversion and linear to circular polarization based on graphene–vanadium dioxide metamaterials. *Opt. Mater.* **2024**, *150*, 115238. [CrossRef]
56. Xiong, T.H.; Zhao, K.; Li, W.; Peng, Y.X.; He, M.D.; Wang, K.J.; Zhang, X.M.; Li, J.B.; Liu, J.Q. Tunable multiband metamaterial coherent perfect absorber based on graphene and vanadium dioxide. *Opt. Commun.* **2022**, *523*, 128691. [CrossRef]